



Thermal Behavior of MHD Stagnation Ternary Nanofluid over a Melting Surface with Joule Heating

Hyder, A.* ^{1,2}, Lim, Y. J. ¹, Khan, I. ³, and Shafie, S. ¹

¹*Department of Mathematical Sciences, Faculty of Science,
Universiti Teknologi Malaysia, 81310 Johor Bahru, Johor, Malaysia*

²*Department of Mathematics and Social Sciences, Sukkur IBA University,
Sukkur 65200, Pakistan*

³*Department of Mathematics, College of Science Al-Zulfi,
Majmaah University, Al-Majmaah 11952, Saudi Arabia*

E-mail: arfanhyder@graduate.utm.my

*Corresponding author

Received: 22 April 2024

Accepted: 4 November 2024

Abstract

The optimal performance of industrial and manufacturing processes, cooling devices, as well as energy storage systems relies on the efficiency of a thermal systems. This study investigates the thermal performance of a ternary hybrid nanofluid consisting of Al_2O_3 , TiO_2 and Cu nanoparticles suspended in water, under the influence of a magnetic field and the phase transition like melting process. The research problem focuses on understanding how the melting parameter, Eckert number and magnetic field strength affect the fluid flow and heat transfer characteristics. The similarity transformation technique is employed to reduce the complexity of the developed governing equations. Then, the simplified governing equations are solved numerically using the Keller-Box method. The findings reveal that the magnetic field increases the temperature profile due to Joule heating, while an increase in the melting parameter inversely affects the temperature profile. The melting parameter enhances the Nusselt number by 35.05% without the magnetic field's influence. The novelty of this study lies in its comprehensive analysis of the interplay between magnetic field, melting parameter and the thermal behavior of ternary hybrid nanofluid, providing valuable guidance for optimizing thermal systems in various industrial applications.

Keywords: ternary hybrid nanofluid; stagnation point; melting heat transfer; joule heating; magnetohydrodynamic; Keller-box method.

List of Abbreviations and Symbols

Al_2O_3	:	Alumina Oxide
Cu	:	Copper
D_1, D_2, D_3, D_4	:	Constants
Ml	:	Melting parameter
$(\cdot)_f$:	Base fluid
$(\cdot)_{hnf}$:	Hybrid nanofluid
$(\cdot)_{thnf}$:	Ternary hybrid nanofluid
ϕ_C	:	Volume fraction of copper
ϕ_A	:	Volume fraction of alumina
T_m	:	Melting surface temperature (K)
T_∞	:	Ambient temperature (K)
T_s	:	Temperature of the solid medium (K)
T_w	:	Temperature of the surface plate (K)
u_e	:	Free stream velocity ($m s^{-1}$)
C_p	:	Specific heat ($J/kg.K$)
Pr	:	Prandtl number
Nu	:	Nusselt number
C_f	:	Skin friction coefficient
Re	:	Reynold's number
Re_x	:	Local Reynold's number
k	:	Thermal conductivity ($W/m.k$)
Mg	:	Magnetic parameter
f	:	Similarity variable
α	:	Thermal diffusivity (m^2/s)
γ	:	A dimensionless small quantity ($\ll 1$)
η	:	Similarity variable
μ	:	Absolute (Dynamic) viscosity (Ns/m^2)
ν	:	Kinematic viscosity (m^2/s)
ρ	:	Density (kg/m^3)
ρC_p	:	Heat capacity (J/m^3K)
ϕ	:	The dimensionless solid volume fraction of hybrid nanofluid
θ	:	Dimensionless temperature
σ	:	Electrical conductivity
δ	:	Boundary layer thickness
τ	:	Shear stress
ψ	:	Stream function
P	:	Pressure (N/m^2)
Ec	:	Eckert number

1 Introduction

In 1995, Choi brought forth an inventive concept known as nanofluid, marking a paradigm shift by integrating nanoparticles into base fluids, thereby unlocking new dimensions in the enhancement of fluid thermal characteristics. Nanofluids, which contain nanoparticles less than 100 nm in size, are consistently and stably dispersed within the base fluid. This stable dispersion leads to improved thermal conductivity and enhanced conduction and convection coefficients, thus facilitating more efficient heat transfer, as reported by Krishna et al. [25] and Kotha et al.

[24]. The advent of this innovation spurred a wave of research, mostly aimed at enhancing the nanofluid's thermal efficiency and heat transfer attributes [11, 13]. The progress of nanofluid reached a turning point with the introduction of hybrid nanofluid, a clever combination involving the addition of another nanoparticle type merged into the base fluid. This mixture, containing two distinct nanoparticles, revealed several novel properties, with the most striking being a considerable rise in thermal conductivity. The discovery of these qualities inspired a fervent desire within the research community to utilize and enhance the capabilities of hybrid nanofluid for practical, real-world applications [20, 18].

To improve the heat-conduction abilities of fluids, the concept of a Ternary Hybrid Nanofluid (THNF) was introduced by Manjunatha et al. [31] representing an evolution from traditional hybrid nanofluids through the incorporation of a three-component mixture. A recent development in nanotechnology is the creation of three-particle nanofluids, which opens up new research opportunities by combining different kinds of nanoparticles to create an optimal nanofluid. THNFs have much greater thermophysical characteristics when compared to standard base or ordinary fluids, along with single-particle and double-particles suspensions. This is due to the combined and powerful effects they exhibit [14]. Scholars are currently studying the traits and behavior of THNFs to determine their advantages, limitations and usability for a range of uses [1]. This tripartite collaboration, including metals, nitrides, metal carbides, oxide ceramics and nonmetals is meticulously dispersed within a chosen base fluid such as water, engine oil, kerosene, or biofluids, among others [45]. This novel blend has captured the interest of researchers not only because of its improved thermal properties but also because of its extensive use in several disciplines, including nanotechnology, solar energy, heat exchangers, automotive cooling systems and biomedical applications. For instance, current research uses micropolar THNF to understand the precise dynamics of blood flow and optimize entropy generation in biomedical contexts, providing revolutionary insights that potentially redefine medical treatments and technology designs [41].

Recent investigations into Magnetohydrodynamics (MHD) and Joule heating of THNF, which is composed of a mixture of nanoparticles like Al_2O_3 (alumina), Cu (copper), and TiO_2 (titania) in water-based fluid, highlight THNF's transformative potential in improving heat transfer rates and energy transmission, thereby setting new benchmarks in the field [37]. This study focuses on a water-based fluid containing Al_2O_3 , TiO_2 and Cu nanoparticles. This decision is supported by their broad use in chemical engineering and the significant interest they have received from the research community. These nanoparticles' unique synergistic effects, particularly when combined in a THNF, provide a multifaceted enhancement in both thermal and mechanical properties, paving the way for novel applications and establishing new frontiers in the constantly evolving field of nanofluid technology [39]. Magnetohydrodynamics, commonly abbreviated as MHD, is the scientific field that explores how electrically conductive fluids, such as liquid crystals, seawater, solitons and electrodes, behave and move.

The name magnetohydrodynamics derives from three words: "magneto" pointing to magnetic fields, "hydro" indicating liquid and "dynamic" signifying motion. In the domain of MHD, magnetic and electric fields interact in a way that can produce electricity, following the principles of Faraday's law of electromagnetic induction. This interaction between the fields can cause electric currents to flow in a fluid that conducts electricity [16]. Joule heating, on the other hand, is a phenomenon in which electric currents passing through a conductor generate heat due to the material's resistance to the flow of electrons [47]. The interaction of Joule heating can greatly influence the characteristics of heat transfer. The localized heating effect of Joule heating can be leveraged to precisely alter melting patterns and phase change kinetics in a variety of applications [19]. Recent studies have illuminated the multifaceted roles of Joule heating in enhancing the thermal performance and operational stability of nanofluids. For instance, the research by Kotha et al. [29] investigates how Joule heating and other parameters affect heat transfer in hy-

brid nanofluid. Similarly, the work by Mohanty et al. [33] underscores the pivotal role of Joule heating in controlling the thermal properties and heat transfer rates in ternary hybrid nanofluid, offering new avenues for thermal management and control in various engineering applications. This dual influence is instrumental in mitigating thermal hotspots and ensuring a more uniform distribution of heat, which is crucial in applications such as electronic cooling, energy storage systems and chemical processing [32, 51]. As the research in this domain continues to evolve, the integration of MHD and Joule heating in melting heat transfer is set to redefine the boundaries of thermal management and energy efficiency, heralding a new era of innovation and technological advancement.

The emerging field of Melting Heat Transfer (MHT) is at the cutting-edge of innovation, providing a beacon of hope in the global struggle for energy sustainability. As researchers delve further into this topic, the combination of MHT, latent thermal energy and phase transition processes reveals a wealth of opportunities for addressing the energy issue. These processes, intricately involved in phase transitions such as solid to liquid or liquid to gas, capture latent energy during phase shifts, opening the way for the development of robust and sustainable energy systems [40]. Because of their ability to store and release large amounts of energy, these systems are necessary for producing solar power, storing thermal energy and utilizing waste heat, helping to advance sustainable energy technologies and reduce the current energy crisis [30]. The spectrum of MHT applications is vast and versatile, encompassing many aspects of modern industry and technology. The phenomenon, first observed by Yen in 1963 [48, 10], has since received attention. This versatility not only promotes improvements in sustainable energy solutions but also propels a wide range of industrial processes into the future [8, 17]. Recent studies in the field of MHT have provided insight into its multidimensional potential and efficiency. Kumar et al. [27] studied melting heat transfer and boundary layer flow while accounting for the impact of Joule heating and found that a greater melting parameter lowers the heat transfer rate. Such findings are extremely important in improving the productivity of energy systems.

Li et al. [28] examined the heat transfer dynamics during melting in a bioconvection magneto-hydrodynamics system, highlighting the complex interactions between thermal radiation and Casson nanofluid under different boundary slip conditions. This work not only broadens the scope of thermal engineering, but also emphasizes potential applications in bioprocessing. Furthermore, the detailed comparison of melting heat transfer in squeezing flow conducted by Muhammad et al. [34] offers a profound understanding of the mathematical intricacies involved in base fluid, nanofluid and hybrid nanofluid dynamics. Such comprehensive studies are instrumental in fine-tuning the theoretical framework and practical implementation of Melting Heat Transfer (MHT) in various industrial and environmental applications, heralding a new era of energy efficiency and technological advancement. The intricate interplay of magnetic fields in MHT provides valuable insights into fluid flow and thermal processes, leading to numerous groundbreaking applications and innovations. Specifically, a real-world application of this study is in enhancing Phase Change Materials (PCMs) for thermal energy storage in renewable energy systems. MHT principles optimize the melting and solidification processes, improving the efficiency of solar energy storage and reducing energy loss [2].

To the best of existing knowledge, the intricate characteristics of ternary hybrid nanofluid, especially concerning melting heat transfer at the stagnation point flow under the influence of Joule heating with MHD, have not been thoroughly investigated. This research addresses a significant gap by exploring the complex interplay between melting heat transfer dynamics and the behavior of ternary hybrid nanofluid at the stagnation point, identifying a comparatively unexplored domain in the existing academic literature. A thorough examination of the melting heat transfer properties of ternary hybrid nanofluid at the stagnation point reveals valuable insights into the thermal behavior of this complex fluid. This study places particular emphasis on their interac-

tions on a horizontal plate under specific fluid flow conditions. This study seeks to bridge the research gap by analyzing how essential factors, such as the melting parameter, magnetic effects and Joule heating, influence temperature and velocity profiles, as well as skin friction and the Nusselt number. The study uses a water-based ternary hybrid nanofluid suspended in alumina (Al_2O_3), copper (Cu) and titanium oxide (TiO_2) nanoparticles. The investigation is not only grounded theoretically but also compared with existing literature on mono-fluid and hybrid nanofluid dynamics, ensuring a thorough and comparative approach. The thoroughly formulated governing equations are dealt with the Keller-Box method, a robust and unconditionally stable numerical methodology that provides precision and reliability in unraveling the complex interactions that characterize such advanced fluid systems.

2 The Governing Equations

This research examines the steady flow of a ternary hybrid nanofluid approaching a horizontal sheet, which exhibits melting properties. The external flow is characterized by a velocity $u_e(x) = ax, a > 0$. The temperature T_m is maintained at the melting surface, while T_∞ represents the free-stream temperature, with $T_\infty > T_m$. Away from the interface, the temperature of the solid medium remains constant at T_s , with $T_s < T_m$ as depicted in Figure 1. Considering a small magnetic Reynolds number and negligible viscous dissipation, the Hall effect and induced magnetic field are neglected. As noted by Krishna et al. [26], the Hall effect significantly impacts the conductivity in ionized gases under strong electric fields, which is not the case in this study. The core equations: governing the system the continuity, momentum and energy equations are adapted from those applicable to ternary hybrid nanofluids by employing boundary layer theory assumptions. The governing equations are Wahid et al. [49],

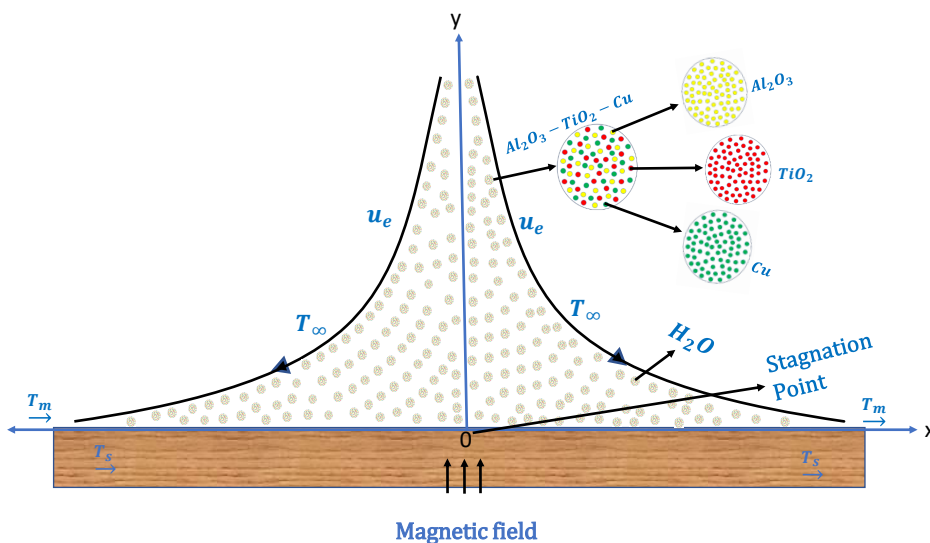


Figure 1: Graphical visualization of the model.

$$\frac{\partial u}{\partial x} + \frac{\partial v}{\partial y} = 0, \quad (1)$$

$$u \frac{\partial u}{\partial x} + v \frac{\partial u}{\partial y} = u_e \frac{du_e}{dx} + \nu_{thnf} \frac{\partial^2 u}{\partial y^2} - \frac{\sigma_{thnf} B_0^2}{\rho_{thnf}} (u - u_e), \quad (2)$$

$$u \frac{\partial T}{\partial x} + v \frac{\partial T}{\partial y} = \frac{k_{thnf}}{\rho_{thnf} (C_p)_{thnf}} \left(\frac{\partial^2 T}{\partial y^2} \right) + \frac{\sigma_{thnf}}{(\rho C_p)_{thnf}} B_0^2 (u - u_e)^2. \quad (3)$$

The flow field velocity is defined in x and y directions, represented as u and v , respectively. Here, the y -axis is defined as perpendicular to the sheet's surface. In this context, the kinematic viscosity of the ternary hybrid nanofluid, represented as ν_{thnf} , is calculated using the formula $\nu_{thnf} = \frac{\mu_{thnf}}{\rho_{thnf}}$. Here, μ_{thnf} refers to the dynamic viscosity and ρ_{thnf} represents the density of the ternary hybrid nanofluid. The symbol σ_{thnf} represents the electrical conductivity of the ternary hybrid nanofluid, while B_0^2 indicates the intensity of the externally applied magnetic field. The temperature within the ternary hybrid nanofluid flow is represented by T . Additionally, k_{thnf} and $(\rho C_p)_{thnf}$ represent the thermal conductivity and heat capacitance of the ternary hybrid nanofluid, respectively.

The boundary conditions associated with (1)–(3) are outlined below [44],

$$\begin{aligned} y = 0 : \quad T &= T_m, \quad u = 0, \\ k_{thnf} \left(\frac{\partial T}{\partial y} \right)_{y=0} &= \rho_{thnf} \left[\lambda + C_s (T_m - T_s) \right] v(x, 0), \\ y \rightarrow \infty : \quad T &= T_\infty, \quad u = u_e(x). \end{aligned} \quad (4)$$

The symbol C_s signifies solid heat capacity and λ denotes latent heat of fluid. According to this, the heat of melting, along with the sensible heat necessary to elevate the solid surface temperature T_s to the melting temperature T_m , is equal to the total amount of heat transferred to the melting surface [9]. To translate (1)–(3) into an ODE system, the appropriate similarity transformations are chosen [52],

$$\psi(x, y) = (a\nu_f)^{1/2} x f(\eta), \quad \theta(\eta) = \frac{T - T_m}{T_\infty - T_m}, \quad \eta = y \left(\frac{a}{\nu_f} \right)^{1/2}. \quad (5)$$

Here, $u = \frac{\partial \psi}{\partial y}$ and $v = -\frac{\partial \psi}{\partial x}$ are defined. When these transformations are applied to equations, the continuity (1) is indeed satisfied and from (2) and (3), the following results are obtained,

$$D_1 f''' + D_2 (f f'' + 1 - f'^2) - D_3 M g (f' - 1) = 0, \quad (6)$$

$$D_4 \theta'' + D_5 Pr f \theta' + D_3 Pr M_g Ec (f' - 1)^2 = 0. \quad (7)$$

The magnetic parameter is $Mg = \frac{\sigma_f B_0^2}{\rho_f a}$. Eckert number is $Ec = \frac{U_e^2(x)}{(C_p)_f (T_\infty - T_m)}$. Pr is the Prantl number, defined as $Pr = \frac{\nu_f}{\alpha_f} = \frac{(\mu C_p)_f}{k_f}$. Primes represent differentiation with respect to η .

Table 1, outlines the thermophysical characteristics of various nanofluid categories, encompassing nanofluid, hybrid nanofluid and THNF. Each category is assessed under a uniform set of parameters. The ϕ indicates the nanoparticle's volume fraction, where $\phi_A = \phi_{Al_2O_3}$, $\phi_C = \phi_{Cu}$ and

$\phi_T = \phi_{TiO_2}$ correspond to the volume fractions of alumina, copper and titanium oxide nanoparticles, respectively. For clarity in distinguishing among the fluid types, a consistent subscript notation is adopted: $(\)_f$ for the base fluid, $(\)_{nf}$ for the nanofluid, $(\)_{hnf}$ for the hybrid nanofluid and $(\)_{thnf}$ for the ternary hybrid nanofluid. The derived constants are as follows,

$$D_1 = \frac{\mu_{thnf}}{\mu_f}, \quad D_2 = \frac{\rho_{thnf}}{\rho_f}, \quad D_3 = \frac{\sigma_{thnf}}{\sigma_f}, \quad D_4 = \frac{k_{thnf}}{k_f}, \quad D_5 = \frac{(\rho C_P)_{thnf}}{(\rho C_P)_f}.$$

The boundary conditions (4) become,

$$\left. \begin{aligned} u(0) = 0, \quad g(0) = 0, \\ D_2 Pr f(0) + D_4 Ml s(0) = 0, \quad \text{at } \eta = 0, \\ u(\eta) = 1, \quad g(\eta) = 1, \quad \text{at } \eta \rightarrow \infty. \end{aligned} \right\} \quad (8)$$

Here, the melting parameter is designated as $Ml = \frac{Cp_f(T_\infty - T_m)}{\lambda + C_s(T_m - T_s)}$. This parameter comprises the Stefan numbers for both solid phases ($C_f(T_\infty - T_m)/\lambda$) and fluid ($C_s(T_m - T_s)/\lambda$) at a constant pressure level. The base fluid's heat capacity is denoted by Cp_f , as noted in [44].

Table 1: Physical properties of the ternary hybrid nanofluid [4, 22, 36].

Mathematical expression for Thermophysical Properties of Nanofluid, Hybrid Nanofluid and Ternary Hybrid Nanofluid.
<p>Dynamic Viscosity:</p> $\mu_{thnf} = \frac{\mu_f}{(1 - \phi_A)^{2.5}(1 - \phi_C)^{2.5}(1 - \phi_T)^{2.5}}.$ $\mu_{hnf} = \frac{\mu_f}{(1 - \phi_T)^{2.5}(1 - \phi_A)^{2.5}}.$ $\mu_{nf} = \frac{\mu_f}{(1 - \phi_T)^{2.5}}.$
<p>Density:</p> $\rho_{thnf} = \left[(1 - \phi_A) \left\{ (1 - \phi_C) \left((1 - \phi_T) \rho_f + \rho_T \phi_T \right) + \rho_C \phi_C \right\} + \rho_A \phi_A \right].$ $\rho_{hnf} = (1 - \phi_A) \left\{ (1 - \phi_T) \rho_f + \rho_T \phi_T \right\} + \rho_A \phi_A.$ $\rho_{nf} = (1 - \phi_T) \rho_f + \rho_T \phi_T.$
<p>Heat Capacity:</p> $(\rho C_P)_{thnf} = \left[(1 - \phi_A) \left\{ (1 - \phi_C) \left((\rho C_P)_f (1 - \phi_T) + (\rho C_P)_T \phi_T \right) + (\rho C_P)_C \phi_C \right\} + (\rho C_P)_A \phi_A \right].$ $(\rho C_P)_{hnf} = (1 - \phi_A) \left\{ (\rho C_P)_f (1 - \phi_T) + (\rho C_P)_T \phi_T \right\} + (\rho C_P)_A \phi_A.$ $(\rho C_P)_{nf} = (\rho C_P)_f (1 - \phi_T) + (\rho C_P)_T \phi_T.$

Thermal Conductivity:

$$\frac{k_{thnf}}{k_{hnf}} = \frac{k_C + 2k_{hnf} - 2\phi_C(k_{hnf} - k_C)}{k_C + 2k_{hnf} + \phi_C(k_{hnf} - k_C)},$$

$$\frac{k_{hnf}}{k_{nf}} = \frac{k_A + 2k_{nf} - 2\phi_A(k_{nf} - k_A)}{k_A + 2k_{nf} + \phi_A(k_{nf} - k_A)},$$

$$\frac{k_{nf}}{k_f} = \frac{k_T + 2k_f - 2\phi_T(k_f - k_T)}{k_T + 2k_f + \phi_T(k_f - k_T)}.$$

Electrical Conductivity:

$$\frac{\sigma_{thnf}}{\sigma_{hnf}} = \frac{\sigma_C(1 + 2\phi_C) + \sigma_{hnf}(1 - 2\phi_C)}{\sigma_C(1 - \phi_C) + \sigma_{hnf}(1 + \phi_C)},$$

$$\frac{\sigma_{hnf}}{\sigma_{nf}} = \frac{\sigma_A(1 + 2\phi_A) + \sigma_{nf}(1 - 2\phi_A)}{\sigma_A(1 - \phi_A) + \sigma_{nf}(1 + \phi_A)},$$

$$\frac{\sigma_{nf}}{\sigma_f} = \frac{\sigma_T(1 + 2\phi_T) + \sigma_f(1 - 2\phi_T)}{\sigma_T(1 - \phi_T) + \sigma_f(1 + \phi_T)}.$$

In the fields of engineering and science, where practical applications abound, a structured mathematical description of the important dimensionless parameters namely, the Nusselt number and the skin friction coefficient represented as Nu and C_f , respectively are as follows,

$$Nu = \frac{xk_{nf}}{k_f(T_\infty - T_m)} \left(\frac{\partial T}{\partial y} \right)_{y=0}, \quad C_f = \frac{\mu_{thnf}}{\rho_f u_e^2} \left(\frac{\partial u}{\partial y} \right)_{y=0}. \quad (9)$$

The local Nusselt number, denoted as Nu_x , is stated below after undergoing simplification [50],

$$Nu_x = \sqrt{Re_x} Nu = -\frac{k_{thnf}}{k_f} \theta'(0) = -D_4 \theta'(0), \quad \because Re_x = \frac{u_e x}{\nu_f}, \quad (10)$$

and local Skin Friction $C_{f,x}$ is defined as follows,

$$C_{f,x} = C_f \sqrt{Re_x} = \frac{\mu_{thnf}}{\mu_f} f''(0) = D_1 f''(0). \quad (11)$$

Table 2: Thermal properties of the base fluid and nanoparticles [37, 6].

Physical Characteristics	Thermal Conductivity k ($Wm^{-1}K^{-1}$)	Specific Heat C_p ($Jkg^{-1}K^{-1}$)	Density ρ (kgm^{-3})	Electrical Conductivity σ (Sm^{-1})
Water (H ₂ O)	0.613	4179	997.1	5.5×10^{-6}
Copper (Cu)	400	385	8933	5.96×10^7
Alumina (Al ₂ O ₃)	40	765	3970	3.5×10^7
Titanium (TiO ₂)	8.9538	686.2	4250	1.0×10^{-18}

3 Numerical Approach: Keller Box Method

The Keller Box method is employed to obtain numerical solutions for the governing equations, with the boundary conditions (8). The process to derive the Keller Box solution involves the subsequent steps.

1. Change (6) and (7) subjected to boundary conditions (8) to a first-order system as,

$$f' = u_1, \quad f'' = u_2, \quad \theta = u_3, \quad \theta' = u_4.$$

2. Here f, u_1, u_2, u_3 and u_4 represent newly developed variables. With respect to these new dependent variables, the system is reformulated to a first-order system as follows,

$$u'_1 = u_2, \tag{12}$$

$$u'_3 = u_4, \tag{13}$$

$$f' = u_1, \tag{14}$$

$$D_1u'_2 + D_2(fu_2 - u_1^2 + 1) + D_3Mg(1 - u_1) = 0, \tag{15}$$

$$D_4u'_4 + D_5Prfu_4 + D_3PrMgEc(u_1 - 1)^2 = 0. \tag{16}$$

The boundary conditions (8) will become,

$$\left. \begin{aligned} u(0) = 0, \quad g(0) = 0, \\ D_4Prf(0) + D_5Mls(0) = 0, \quad \text{at } \eta = 0. \\ u(\eta) = 1, \quad g(\eta) = 1, \quad \text{at } \eta \rightarrow \infty. \end{aligned} \right\} \tag{17}$$

3. The system is converted into a nonlinear algebraic system through the application of centered finite difference derivatives. In this specific case, attention is solely on the η -plane within the defined rectangular network. The net points are established as below,

$$\eta^0 = 0, \quad \eta_j = \eta_{j-1} + h_j, \quad j = 1, 2, \dots, J, \quad \eta_J \equiv \eta_\infty.$$

Here, h_j represents the spacing in $\Delta\eta$ and the coordinate positions are indicated by integers

j . The derivatives along the η -direction are generally known as $q' = \frac{\partial q}{\partial \eta} = \frac{q_j - q_{j-1}}{h_j}$ and

similarly, $p_{j-1/2} = \frac{p_j + p_{j-1}}{2}$, applicable across all general points in the network.

4. Apply Newton’s method to linearize the nonlinear system,

$$()^{(i+1)}_j = ()^{(i)}_j + \delta()^{(i)}_j, \quad \text{where } i = 0, 1, 2, 3, \dots \tag{18}$$

Upon substituting this into (12)–(16) and for simplicity, the superscript i and terms of order two or higher in $\delta f^{(i)}_j, \delta u^{(i)}_j, \delta v^{(i)}_j, \delta s^{(i)}_j$, and $\delta g^{(i)}_j$ are omitted. This results in the derivation of a linear tridiagonal system as follows:

$$\delta u_j - \delta u_{j-1} - \frac{h_j}{2}(\delta v_j + \delta v_{j-1}) = (r_1)_{j-1/2}, \tag{19}$$

$$\delta g_j - \delta g_{j-1} - \frac{h_j}{2}(\delta s_j + \delta s_{j-1}) = (r_2)_{j-1/2}, \tag{20}$$

$$\delta f_j - \delta f_{j-1} - \frac{h_j}{2}(\delta u_j + \delta u_{j-1}) = (r_3)_{j-1/2}, \tag{21}$$

$$(a_1)_j \delta v_j + (a_2)_j \delta v_{j-1} + (a_3)_j \delta f_j + (a_4)_j \delta f_{j-1} + (a_5)_j \delta u_j + (a_6)_j \delta u_{j-1} = (r_4)_{j-1/2}, \tag{22}$$

$$(b_1)_j \delta s_j + (b_2)_j \delta s_{j-1} + (b_3)_j \delta f_j + (b_4)_j \delta f_{j-1} + (b_5)_j \delta u_j + (b_6)_j \delta u_{j-1} = (r_5)_{j-1/2}, \tag{23}$$

where

$$\left. \begin{aligned} (a_1)_j &= D_1 + \frac{h_j}{2} D_2 f_{j-1/2}, \\ (a_2)_j &= \frac{h_j}{2} D_2 f_{j-1/2} - D_1, \\ (a_3)_j &= (a_4)_j = \frac{h_j}{2} D_2 v_{j-1/2}, \\ (a_5)_j &= (a_6)_j = -D_2 h_j u_{j-1/2} - \frac{h_j}{2} D_3 M g. \end{aligned} \right\} \tag{24}$$

$$\left. \begin{aligned} (b_1)_j &= D_4 + \frac{h_j}{2} D_5 Pr f_{j-1/2}, \\ (b_2)_j &= \frac{h_j}{2} D_5 Pr f_{j-1/2} - D_4, \\ (b_3)_j &= (b_4)_j = \frac{h_j}{2} D_5 Pr s_{j-1/2}, \\ (b_5)_j &= (b_6)_j = D_3 h_j Pr M_g Ec(u_{j-1/2}) - D_3 h_j Pr M_g Ec. \end{aligned} \right\} \tag{25}$$

$$\left. \begin{aligned} (r_1)_{j-1/2} &= u_{j-1} - u_j + h_j v_{j-1/2}, \\ (r_2)_{j-1/2} &= g_{j-1} - g_j + h_j s_{j-1/2}, \\ (r_3)_{j-1/2} &= f_{j-1} - f_j + h_j u_{j-1/2}, \\ (r_4)_{j-1/2} &= D_1(v_{j-1} - v_j) - h_j D_2 v_{j-1/2} f_{j-1/2} + h_j D_2 (u_{j-1/2})^2 \\ &\quad + h_j D_3 M g u_{j-1/2} - h_j (D_2 + D_3 M g), \\ (r_5)_{j-1/2} &= D_4 (s_{j-1} - s_j) - h_j Pr D_5 s_{j-1/2} f_{j-1/2} - \\ &\quad D_3 h_j Pr M_g Ec(u_{j-1/2})^2 + 2 D_3 h_j Pr M_g Ec(u_{j-1/2}) - D_3 h_j Pr M_g Ec. \end{aligned} \right\} \tag{26}$$

While using (35), the boundary conditions (17) are written as follows,

$$\delta u_0 = 0, \quad \delta g_0 = 0, \quad D_2 Pr \delta f_0 + D_4 M l \delta s_0 = 0, \quad \delta u_J = 0, \quad \delta g_J = 0. \tag{27}$$

Table 3: Validation of melting parameters, $f''(0)$ and $-\theta'(0)$ in comparison with existing literature, holding other parameters at zero and setting $Pr = 1$.

Me	Pop et al. [35]		Current work	
	$f''(0)$	$-\theta'(0)$	$f''(0)$	$-\theta'(0)$
0	1.2325876	-0.5704652	1.2325976	-0.5704689
1	1.0370034	-0.3619611	1.0370111	-0.3619628
2	0.9468506	-0.2737027	0.9468574	-0.2737037
3	0.8913811	-0.2231390	0.8913875	-0.2231396

Table 4: Certain chosen values of C_{fx} and Nu_x are considered, with a variety of parameters, while maintaining $Pr = 6.2$ and setting $\phi_C = \phi_A = \phi_T = 0.01$.

MI	Mg	Ec	C_{fx}	Nu_x
1	1	0	1.5682	-3.5793
		1	1.5871	-1.8403
		2	1.5116	-2.785
2	1	1	1.4982	-1.4791
	2		1.7143	-2.128
	3		1.9094	-2.6563
1	1	1	1.5871	-1.8403
2			1.4982	-1.4791
3			1.4324	-1.2749

5. The linearized differential equations are solved employing the block tridiagonal elimination method.

Equations (19) to (23), which are expressed as,

$$\begin{bmatrix} [A_1] & [C_1] & & & & & \\ [B_2] & [A_2] & [C_2] & & & & \\ & & & \ddots & & & \\ & & & & \ddots & & \\ & & & & & \ddots & \\ & & [B_{J-1}] & [A_{J-1}] & [C_{J-1}] & & \\ & & & [B_J] & [A_J] & & \end{bmatrix} \begin{bmatrix} [\delta_1] \\ [\delta_2] \\ [\delta_3] \\ \vdots \\ [\delta_{J-1}] \\ [\delta_J] \end{bmatrix} = \begin{bmatrix} [r_1] \\ [r_2] \\ [r_3] \\ \vdots \\ [r_{J-1}] \\ [r_J] \end{bmatrix}, \tag{28}$$

or

$$[A][\delta] = [r]. \tag{29}$$

The elements of the matrices are given by,

$$[A_j] = \begin{bmatrix} 1 & -h_j/2 & 0 & 0 & 0 \\ (a_3)_{j-1} & (a_5)_{j-1} & (a_1)_{j-1} & 0 & 0 \\ (b_3)_{j-1} & (b_5)_{j-1} & 0 & 0 & (b_1)_{j-1} \\ 0 & -1 & -h_j/2 & 0 & 0 \\ 0 & 0 & 0 & -1 & -h_j/2 \end{bmatrix}, \quad \text{where } 2 \leq j \leq J - 1. \tag{30}$$

$$[C_j] = \begin{bmatrix} 0 & 0 & 0 & 0 & 0 \\ 0 & 0 & 0 & 0 & 0 \\ 0 & 0 & 0 & 0 & 0 \\ 0 & 1 & -h_j/2 & 0 & 0 \\ 0 & 0 & 0 & 1 & -h_j/2 \end{bmatrix}, \quad \text{where } 1 \leq j \leq J - 1. \tag{31}$$

$$[B_j] = \begin{bmatrix} -1 & -h_j/2 & 0 & 0 & 0 \\ (a_4)_{j-1} & (a_6)_{j-1} & (a_2)_{j-1} & 0 & 0 \\ (b_4)_{j-1} & (b_6)_{j-1} & 0 & 0 & (b_2)_{j-1} \\ 0 & 0 & 0 & 0 & 0 \\ 0 & 0 & 0 & 0 & 0 \end{bmatrix}, \quad \text{where } 2 \leq j \leq J. \tag{32}$$

$$[\delta_j] = \begin{bmatrix} \delta f_{j-1} \\ \delta u_{j-1} \\ \delta v_{j-1} \\ \delta g_{j-1} \\ \delta s_{j-1} \end{bmatrix}, \quad \text{where } 1 \leq j \leq J. \quad (33)$$

$$[r_j] = \begin{bmatrix} (r_1)_{j-1/2} \\ (r_2)_{j-1/2} \\ (r_3)_{j-1/2} \\ (r_4)_{j-1/2} \\ (r_5)_{j-1/2} \end{bmatrix}, \quad \text{where } 2 \leq j \leq J - 1. \quad (34)$$

The step size $\Delta y = 0.001 = h$ is used and the process of calculation repeats till the convergence requirement, $|\delta v_0^{(i)}| < \gamma$, is met. γ denotes a moderate set value. $\gamma = 0.00001$ or 10^{-5} is proposed as the convergence limit. The following initial guesses serve as the starting point for the computation,

$$f_0(\eta) = \eta + e^{-\eta} - 1 - \frac{D_4 M}{D_2 P r}, \quad \theta_0(\eta) = u_3(\eta)_0 = 1 - e^{-\eta}. \quad (35)$$

4 Results and Discussion

This study examines the effects of magnetic and melting parameters on water-based ternary hybrid nanofluids. Each nanoparticle, TiO_2 , Al_2O_3 and Cu , contributed 1% to the composition of the ternary hybrid fluid. Our selection of parameters aligns with trends and findings commonly observed in the existing literature [5, 7]. Using MATLAB and the Keller Box technique, computations for the given equations with boundary conditions are performed. Table 2 presents the physical characteristics (constants) of the base fluid and nanoparticles, while Table 1 outlines the mathematical formulation details for the ternary hybrid nanofluid investigated in this study. The validation of the current results is presented in Table 3, which demonstrates their agreement with existing literature. This confirms the accurate implementation of the method.

Figure 2 illustrates how the skin friction coefficient (C_{fx}) and the local Nusselt number ($-Nu_x$) respond to changes in the melting parameter (Ml). Notably, a decrease in Ml leads to a reduction in C_{fx} . Similarly, $-Nu_x$ tends to drop as Ml increases. A negative Nu_x signifies that heat flows from the warmer fluid to the cooler solid surface. When focusing on the absolute value of Nu_x , it becomes clear that an increase in Ml corresponds to a lower heat transfer rate. This behavior is due to the combined effects of reduced shear stress from the melt layer and the substantial heat absorption during the melting process. Similar results are observed in the studies of Sheikholeslami et al. [43] and Khashiie et al. [23].

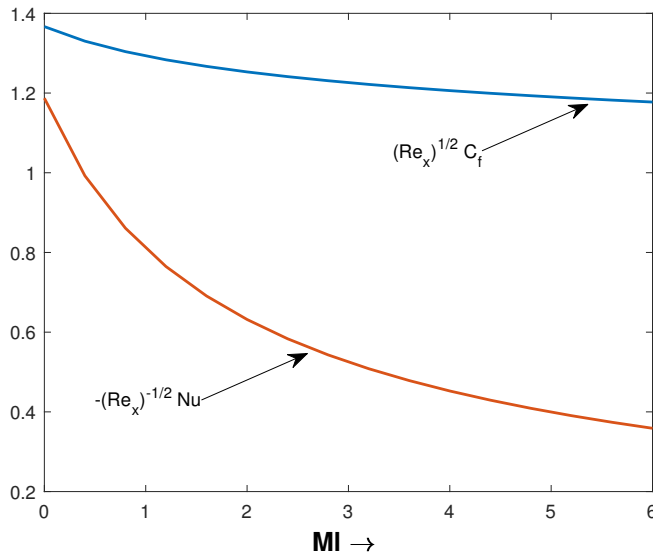


Figure 2: Variation of the local skin friction coefficient (C_{fx}) and local Nusselt number (Nu_x) with the melting parameter (MI).

Figures 3 and 4 show a significant decline in velocity profiles ($f'(\eta)$) and temperature profiles ($\theta(\eta)$) with the rise of the melting parameter (MI). This behavior stems from the primary reason: a higher melting parameter means more molecular activity and phase change within the ternary nanofluid. This, in turn, impedes the dispersion of momentum within the boundary layer, affecting both momentum and thermal diffusion. This results in cooler and slower fluid flow, along with a thinner thermal boundary layer. Furthermore, when comparing a Newtonian fluid such as water to THNF, Figure 3 demonstrates that the velocity profiles of the base fluid are lower than those of THNF. This observation is consistent with the findings of Chu et al. [12]. Additionally, Figure 4 illustrates that the temperature profiles of THNF are lower than those of the base fluid. Physically, this suggests that the higher thermal conductivity of THNF facilitates more efficient temperature transfer during the melting process, resulting in lower temperatures for THNF. This finding aligns with the current state of the art, where THNF is extensively utilized as a cooling agent in various applications, a result also supported by the recent study by Sharma and Badak [42]. Moreover, the enhanced thermal conductivity of THNF leads to a larger temperature gradient, which in turn induces faster fluid movement, as shown in Figure 3.

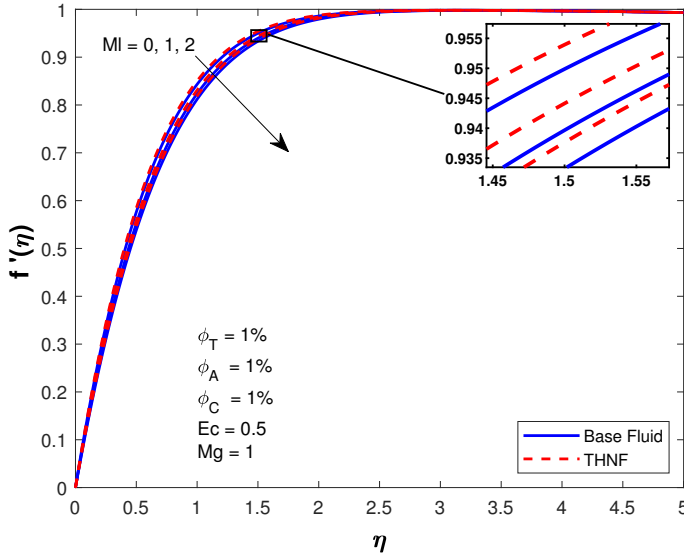


Figure 3: Behavior of velocity profiles ($f'(\eta)$) with respect to the melting parameter (MI).

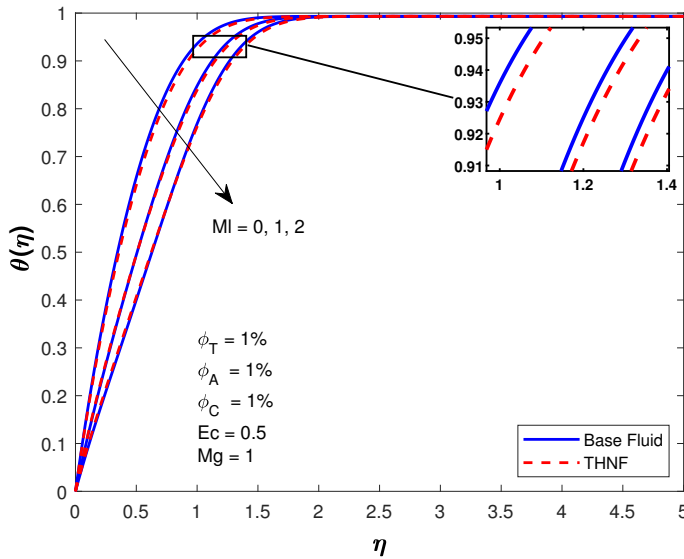


Figure 4: Behavior of temperature profiles ($\theta(\eta)$) with respect to the melting parameter (MI).

Figures 5 and 6 vividly illustrate the clear impact of the increasing magnetic parameter (Mg) on the velocity ($f'(\eta)$) and temperature ($\theta(\eta)$) profiles. As Mg increases, the magnetic field strengthens, leading to a more potent Lorentz force. This force directly influences the velocity profile by affecting the momentum of the fluid particles and also alters the temperature profile by reducing the thickness of the thermal boundary layer on the sheet. Additionally, Joule heating generates energy to counter the effects of the enhanced Lorentz force and friction, resulting in an overall rise in both the temperature and velocity profiles.

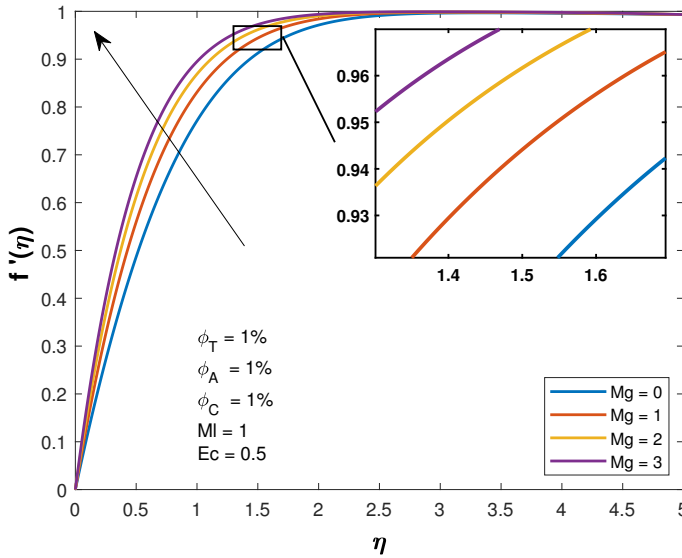


Figure 5: Behavior of velocity profiles ($f'(\eta)$) with respect to the magnetic parameter (Mg).

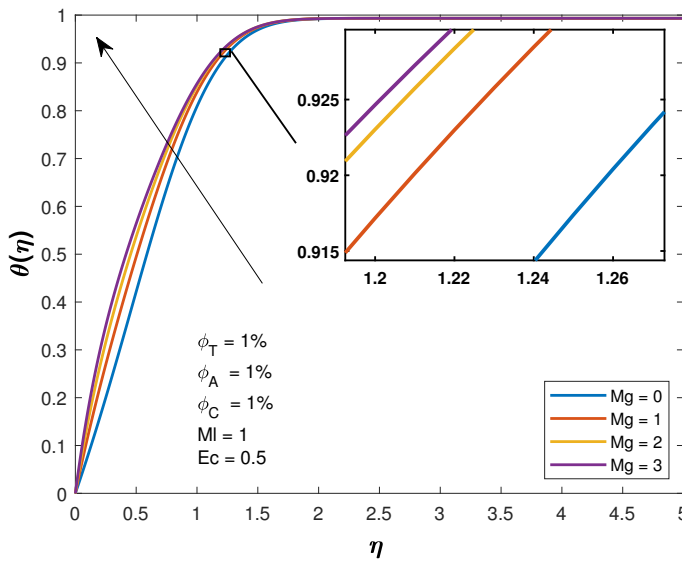


Figure 6: Behavior of temperature profiles ($\theta(\eta)$) with respect to the magnetic parameter (Mg).

Lastly, Figure 7 and Figure 8 demonstrate the correlation between Ec and the fluid’s dynamics. As Ec rises, the velocity profile ($f'(\eta)$) tends to decrease, while the temperature profile ($\theta(\eta)$) increases, a trend also noted by Ramya et al. [38] and Hayat et al. [15]. This phenomenon can be attributed to the internal molecular friction that converts mechanical energy into heat, leading to heightened temperature and reduced velocity in the fluid, as described by Srinivasacharya and Jagadeeshwar [46].

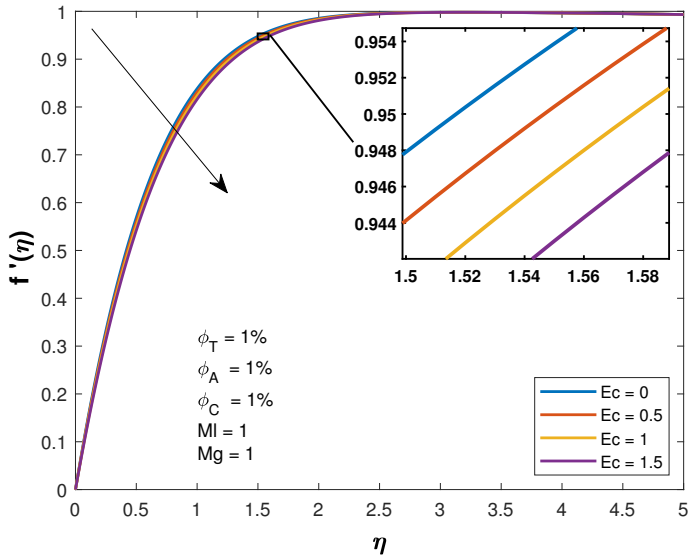


Figure 7: Behavior of velocity profiles ($f'(\eta)$) with the Eckert parameter (Ec).

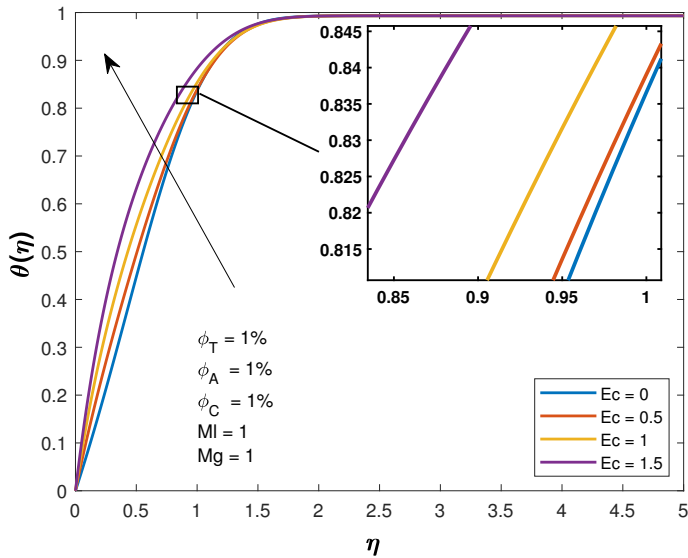


Figure 8: Behavior of temperature profiles ($\theta(\eta)$) with respect to the Eckert parameter (Ec).

5 Conclusion

This research delved into the influence of MHT and Joule heating on the stagnation point flow over a horizontal sheet. The study centers its attention on a ternary hybrid nanofluid composed of Cu, Al₂O₃, TiO₂ nanoparticles dispersed in water, examining its behavior under steady laminar two-dimensional boundary layer conditions. Moreover, this study aims to determine the skin friction coefficient (C_{fx}) and the local Nusselt number (Nu_x), which characterize the frictional and

heat transfer characteristics of a surface. The investigation considers the influence of various parameters that affect these coefficients. The Keller Box technique, a numerical method, is employed to perform computations. The findings are analyzed across several parametric scenarios, leading to noteworthy conclusions:

- A rise in the melting parameter (Ml) value is accompanied by a significant decrease in the heat transfer rate ($-Nu_x$).
- An increase in the Ml results in a decrease in both the velocity profiles (f') and the temperature profiles (θ).
- The magnetic parameter (Mg) is found to enhance both the velocity profiles ($f'(\eta)$) and the temperature profiles ($\theta(\eta)$) due to the Joule heating.
- The Eckert parameter (Ec) is associated with an increase in the temperature profiles ($\theta(\eta)$).
- Conversely, the Eckert parameter (Ec) is linked to a decrease in the velocity profiles ($f'(\eta)$).

This research offers pivotal insights into the behavior of Cu-Al₂O₃-TiO₂/water-based ternary hybrid nanofluid in heat transfer scenarios, emphasizing contexts that involve magnetic fields, melting heat transfer and especially Joule heating effects. Understanding the roles of parameters like the melting parameter, magnetic parameter (Mg) and Eckert number (Ec) paves the way for optimizing thermal processes across various engineering domains. The significance of the Eckert number is particularly notable in the analysis of thermal behavior and velocity changes in nanofluid flows [3], as well as in the optimization of cooling efficiency in CPU systems, where it aids in evaluating heat transfer efficiency [21].

Moreover, the application of ternary hybrid nanofluids in cooling systems, for instance in high-performance electronics or in industries striving for efficient thermal management, can leverage these insights for enhanced heat transfer, resulting in superior device performance and longevity. The detailed observations regarding heat transfer rates and temperature profiles are invaluable, offering a compass for industries focused on optimizing energy use and improving thermal control. These results highlight the capacity of customized ternary hybrid nanofluid compositions and deliberate adjustments of parameters to improve the effectiveness of heat transfer in practical applications, signifying a step forward towards increased energy efficiency and operational performance.

Reflecting on future trends, the study can be enhanced by including thermal radiation effects, modifying the geometry, especially focusing on shrinking and stretching sheets. Future research could critically evaluate the impact of all parameters by comparing nanofluids, hybrid nanofluids and ternary hybrid nanofluids, thereby maximizing the utility of THNF outcomes.

Acknowledgement This research was funded by the Universiti Teknologi Malaysia (UTM), UTM Fundamental Research Vote No: Q.J130000.3854.23H22 and UTM Fundamental Research Vote No: Q.J130000.3854.23H57.

Conflicts of Interest The authors declare no conflict of interest.

References

- [1] H. Adun, D. Kavaz & M. Dagbasi (2021). Review of ternary hybrid nanofluid: Synthesis, stability, thermophysical properties, heat transfer applications, and environmental effects. *Journal of Cleaner Production*, 328, Article ID: 129525. <https://doi.org/10.1016/j.jclepro.2021.129525>.
- [2] F. Agyenim, N. Hewitt, P. Eames & M. Smyth (2010). A review of materials, heat transfer and phase change problem formulation for latent heat thermal energy storage systems (LHTESS). *Renewable and Sustainable Energy Reviews*, 14(2), 615–628. <https://doi.org/10.1016/j.rser.2009.10.015>.
- [3] M. A. Aiyashi, S. M. Abo-Dahab & M. D. Albalwi (2023). Effect of viscous dissipation and induced magnetic field on an unsteady mixed convective stagnation point flow of a nonhomogenous nanofluid. *Scientific Reports*, 13(1), Article ID: 22529. <https://doi.org/10.1038/s41598-023-42593-1>.
- [4] K. F. Al Oweidi, F. Shahzad, W. Jamshed, Usman, R. W. Ibrahim, E. S. M. T. El Din & A. M. AlDerea (2022). Partial differential equations of entropy analysis on ternary hybridity nanofluid flow model via rotating disk with hall current and electromagnetic radiative influences. *Scientific Reports*, 12(1), Article ID: 20692. <https://doi.org/10.1038/s41598-022-24895-y>.
- [5] E. A. Algehyne, Z. Raizah, T. Gul, A. Saeed, S. M. Eldin & A. M. Galal (2023). Cu and Al₂O₃-based hybrid nanofluid flow through a porous cavity. *Nanotechnology Reviews*, 12(1), Article ID: 20220526. <https://doi.org/10.1515/ntrev-2022-0526>.
- [6] B. Ali, I. Siddique, H. Ahmad & S. Askar (2023). Influence of nanoparticles aggregation and Lorentz force on the dynamics of water-titanium dioxide nanoparticles on a rotating surface using finite element simulation. *Scientific Reports*, 13(1), Article ID: 4702. <https://doi.org/10.1038/s41598-023-31771-w>.
- [7] H. M. Ali, M. U. Sajid & A. Arshad (2017). Heat transfer applications of TiO₂ nanofluids. In M. Janus (Ed.), *Application of Titanium Dioxide*, chapter 9, pp. 181–206. IntechOpen, Rijeka. <https://doi.org/10.5772/intechopen.68602>.
- [8] M. S. Alqarni, S. Yasmin, H. Waqas & S. A. Khan (2022). Recent progress in melting heat phenomenon for bioconvection transport of nanofluid through a lubricated surface with swimming microorganisms. *Scientific Reports*, 12(1), Article ID: 8447. <https://doi.org/10.1038/s41598-022-12230-4>.
- [9] A. J. Chamkha, A. M. Rashad & E. Al-Meshaie (2011). Melting effect on unsteady hydro-magnetic flow of a nanofluid past a stretching sheet. *International Journal of Chemical Reactor Engineering*, 9(1), 1–8. <https://doi.org/10.2202/1542-6580.2613>.
- [10] K. C. Cheng & Y. C. Yen (1991). Historical and recent developments in the research of cold regions heat transfer - ice in air, water and earth. In *Freezing and Melting Heat Transfer in Engineering: Selected Topics on Ice-Water Systems and Welding and Casting Processes*, volume 3 pp. 17–63. Hemisphere Publishing Corporation, United States.
- [11] S. U. S. Choi & J. A. Eastman (1995). Enhancing thermal conductivity of fluids with nanoparticles. In *Proceedings of the ASME International Mechanical Engineering Congress and Exposition*, volume 66 pp. 1–8. San Francisco, California.

- [12] Y. M. Chu, S. Bashir, M. Ramzan & M. Y. Malik (2023). Model-based comparative study of magnetohydrodynamics unsteady hybrid nanofluid flow between two infinite parallel plates with particle shape effects. *Mathematical Methods in the Applied Sciences*, 46(10), 11568–11582. <https://doi.org/10.1002/mma.8234>.
- [13] N. A. N. N. Habib, N. S. Arifin, S. M. Zokri & A. R. M. Kasim (2024). MHD flow of dusty jeffrey fluid flow containing carbon nano tubes (CNTs) under influences of viscous dissipation and Newtonian heating. *Malaysian Journal of Mathematical Sciences*, 18(2), 445–468. <https://doi.org/10.47836/mjms.18.2.13>.
- [14] H. Hanif, S. Shafie & Z. T. Jagun (2024). Maximizing heat transfer and minimizing entropy generation in concentric cylinders with CuO-MgO-TiO₂ nanoparticles. *Chinese Journal of Physics*, 89, 493–503. <https://doi.org/10.1016/j.cjph.2023.12.021>.
- [15] T. Hayat, G. Bashir, M. Waqas & A. Alsaedi (2016). MHD flow of Jeffrey liquid due to a nonlinear radially stretched sheet in presence of Newtonian heating. *Results in Physics*, 6, 817–823. <https://doi.org/10.1016/j.rinp.2016.10.001>.
- [16] S. Hussain, K. Rasheed, A. Ali, N. Vrinceanu, A. Alshehri & Z. Shah (2022). A sensitivity analysis of MHD nanofluid flow across an exponentially stretched surface with non-uniform heat flux by response surface methodology. *Scientific Reports*, 12(1), Article ID: 18523. <https://doi.org/10.1038/s41598-022-22970-y>.
- [17] A. Hyder, Y. J. Lim, I. Khan & S. Shafie (2023). Unveiling the performance of Cu–water nanofluid flow with melting heat transfer, MHD, and thermal radiation over a stretching/shrinking sheet. *ACS Omega*, 8(32), 29424–29436. <https://doi.org/10.1021/acsomega.3c02949>.
- [18] A. Hyder, Y. J. Lim, I. Khan & S. Shafie (2024). Investigating heat transfer characteristics in nanofluid and hybrid nanofluid across melting stretching/shrinking boundaries. *Bio-NanoScience*, 14(2), 1181–1195. <https://doi.org/10.1007/s12668-024-01309-z>.
- [19] M. Imran, Z. Abbas, M. Naveed & N. Salamat (2021). Impact of Joule heating and melting on time-dependent flow of nanoparticles due to an oscillatory stretchable curved wall. *Alexandria Engineering Journal*, 60(4), 4097–4113. <https://doi.org/10.1016/j.aej.2021.02.055>.
- [20] S. S. P. M. Isa, S. Parvin, N. Arifin, F. Ali & K. Ahmad (2023). Soret-Dufour effects on the waterbased hybrid nanofluid flow with nanoparticles of Alumina and Copper. *Malaysian Journal of Mathematical Sciences*, 17(3), 283–304. <https://doi.org/10.47836/mjms.17.3.04>.
- [21] A. A. Izadi & H. Rasam (2024). Thermal management of the central processing unit cooling system using a cylindrical metal foam heat sink under the influence of magnetohydrodynamic nanofluid flow. *International Journal of Numerical Methods for Heat & Fluid Flow*, 34(1), 1–30. <http://dx.doi.org/10.1108/HFF-04-2023-0188>.
- [22] S. A. Khan, T. Hayat & A. Alsaedi (2022). Thermal conductivity performance for ternary hybrid nanomaterial subject to entropy generation. *Energy Reports*, 8, 9997–10005. <https://doi.org/10.1016/j.egy.2022.07.149>.
- [23] N. S. Khashi'ie, N. Md Arifin, I. Pop & R. Nazar (2022). Melting heat transfer in hybrid nanofluid flow along a moving surface. *Journal of Thermal Analysis and Calorimetry*, 147(1), 567–578. <https://doi.org/10.1007/s10973-020-10238-4>.
- [24] G. Kotha, V. R. Kolipaula, M. Venkata Subba Rao, S. Penki & A. J. Chamkha (2020). Internal heat generation on bioconvection of an MHD nanofluid flow due to gyrotactic microorganisms. *The European Physical Journal Plus*, 135, Article ID: 600. <https://doi.org/10.1140/epjp/s13360-020-00606-2>.

- [25] M. V. Krishna, N. A. Ahammad & A. J. Chamkha (2021). Radiative MHD flow of Casson hybrid nanofluid over an infinite exponentially accelerated vertical porous surface. *Case Studies in Thermal Engineering*, 27, Article ID: 101229. <https://doi.org/10.1016/j.csite.2021.101229>.
- [26] M. V. Krishna, B. Swarnalathamma & A. J. Chamkha (2019). Investigations of Soret, Joule and Hall effects on MHD rotating mixed convective flow past an infinite vertical porous plate. *Journal of Ocean Engineering and Science*, 4(3), 263–275. <https://doi.org/10.1016/j.joes.2019.05.002>.
- [27] K. G. Kumar, M. R. Krishnamurthy & N. G. Rudraswamy (2019). Boundary layer flow and melting heat transfer of Prandtl fluid over a stretching surface by considering Joule heating effect. *Multidiscipline Modeling in Materials and Structures*, 15(2), 337–352. <https://doi.org/10.1108/MMMS-03-2018-0055>.
- [28] Y. Li, A. Majeed, N. Ijaz, K. Barghout, M. R. Ali & T. Muhammad (2023). Melting thermal transportation in bioconvection Casson nanofluid flow over a nonlinear surface with motile microorganism: Application in bioprocessing thermal engineering. *Case Studies in Thermal Engineering*, 49, Article ID: 103285. <https://doi.org/10.1016/j.csite.2023.103285>.
- [29] L. A. Lund, A. Asghar, G. Rasool & U. Yashkun (2023). Magnetized Casson SA-hybrid nanofluid flow over a permeable moving surface with thermal radiation and Joule heating effect. *Case Studies in Thermal Engineering*, 50, Article ID: 103510. <https://doi.org/10.1016/j.csite.2023.103510>.
- [30] F. Ma, L. Liu, L. Ma, Q. Zhang, J. Li, M. Jing & W. Tan (2022). Enhanced thermal energy storage performance of hydrous salt phase change material via defective graphene. *Journal of Energy Storage*, 48, Article ID: 104064. <https://doi.org/10.1016/j.est.2022.104064>.
- [31] S. Manjunatha, V. Puneeth, B. J. Gireesha & A. J. Chamkha (2022). Theoretical study of convective heat transfer in ternary nanofluid flowing past a stretching sheet. *Journal of Applied and Computational Mechanics*, 8(4), 1279–1286. <https://doi.org/10.22055/jacm.2021.37698.3067>.
- [32] J. Mng'ang'a (2023). Effects of chemical reaction and Joule heating on MHD generalized Couette flow between two parallel vertical porous plates with induced magnetic field and Newtonian heating/cooling. *International Journal of Mathematics and Mathematical Sciences*, 2023(1), Article ID: 9134811. <https://doi.org/10.1155/2023/9134811>.
- [33] D. Mohanty, G. Mahanta & S. Shaw (2024). Irreversibility and thermal performance of nonlinear radiative cross-ternary hybrid nanofluid flow about a stretching cylinder with industrial applications. *Powder Technology*, 433, Article ID: 119255. <https://doi.org/10.1016/j.powtec.2023.119255>.
- [34] K. Muhammad, T. Hayat, A. Alsaedi & B. Ahmad (2021). Melting heat transfer in squeezing flow of basefluid (water), nanofluid (CNTs+ water) and hybrid nanofluid (CNTs+ CuO+ water). *Journal of Thermal Analysis and Calorimetry*, 143, 1157–1174. <https://doi.org/10.1007/s10973-020-09391-7>.
- [35] I. Pop, I. Waini & A. Ishak (2022). MHD stagnation point flow on a shrinking surface with hybrid nanoparticles and melting phenomenon effects. *International Journal of Numerical Methods for Heat & Fluid Flow*, 32(5), 1728–1741. <https://doi.org/10.1108/HFF-06-2021-0378>.
- [36] D. G. Prakasha, M. V. V. N. L. Sudharani, K. G. Kumar & A. J. Chamkha (2023). Comparative study of hybrid (graphene/magnesium oxide) and ternary hybrid (graphene/zirconium oxide/magnesium oxide) nanomaterials over a moving plate. *International Communications in Heat and Mass Transfer*, 140, Article ID: 106557. <https://doi.org/10.1016/j.icheatmasstransfer.2022.106557>.

- [37] K. Rafique, Z. Mahmood, U. Khan, S. M. Eldin, M. Oreijah, K. Guedri & H. A. E. W. Khalifa (2023). Investigation of thermal stratification with velocity slip and variable viscosity on MHD flow of $\text{Al}_2\text{O}_3\text{-Cu-TiO}_2/\text{H}_2\text{O}$ nanofluid over disk. *Case Studies in Thermal Engineering*, 49, Article ID: 103292. <https://doi.org/10.1016/j.csite.2023.103292>.
- [38] D. Ramya, R. S. Raju, J. A. Rao & A. J. Chamkha (2018). Effects of velocity and thermal wall slip on magnetohydrodynamics (MHD) boundary layer viscous flow and heat transfer of a nanofluid over a non-linearly-stretching sheet: A numerical study. *Propulsion and Power Research*, 7(2), 182–195. <https://doi.org/10.1016/j.jprr.2018.04.003>.
- [39] S. Saranya, F. Z. Duraihem, I. L. Animasaun & Q. M. Al-Mdallal (2023). Quartic autocatalysis on horizontal surfaces with an asymmetric concentration: Water-based ternary-hybrid nanofluid carrying titania, copper, and alumina nanoparticles. *Physica Scripta*, 98(7), Article ID: 075214. <https://doi.org/10.1088/1402-4896/acdb08>.
- [40] K. P. Sarath, M. F. Osman, R. Mukhesh, K. V. Manu & M. Deepu (2023). A review of the recent advances in the heat transfer physics in latent heat storage systems. *Thermal Science and Engineering Progress*, 42, Article ID: 101886. <https://doi.org/10.1016/j.tsep.2023.101886>.
- [41] B. K. Sharma, P. Sharma, N. K. Mishra, S. Noeiaghdam & U. Fernandez-Gamiz (2023). Bayesian regularization networks for micropolar ternary hybrid nanofluid flow of blood with homogeneous and heterogeneous reactions: Entropy generation optimization. *Alexandria Engineering Journal*, 77, 127–148. <https://doi.org/10.1016/j.aej.2023.06.080>.
- [42] R. P. Sharma & K. Badak (2024). Heat transport of radiative ternary hybrid nanofluid over a convective stretching sheet with induced magnetic field and heat source/sink. *Journal of Thermal Analysis and Calorimetry*, 149(9), 3877–3889. <https://doi.org/10.1007/s10973-024-12979-y>.
- [43] M. Sheikholeslami, M. Nimafar & D. D. Ganji (2017). Analytical approach for the effect of melting heat transfer on nanofluid heat transfer. *The European Physical Journal Plus*, 132, Article ID: 385. <https://doi.org/10.1140/epjp/i2017-11669-3>.
- [44] K. Singh, A. K. Pandey & M. Kumar (2021). Numerical solution of micropolar fluid flow via stretchable surface with chemical reaction and melting heat transfer using Keller–Box method. *Propulsion and Power Research*, 10(2), 194–207. <https://doi.org/10.1016/j.jprr.2020.11.006>.
- [45] G. F. Smaisim, D. B. Mohammed, A. M. Abdulhadi, K. F. Uktamov, F. H. Alsultany, S. E. Izzat, M. J. Ansari, H. H. Kzar, M. E. Al-Gazally & E. Kianfar (2022). RETRACTED ARTICLE: Nanofluids: properties and applications. *Journal of Sol-Gel Science and Technology*, 104(1), 1–35. <https://doi.org/10.1007/s10971-022-05859-0>.
- [46] D. Srinivasacharya & P. Jagadeeshwar (2019). Effect of Joule heating on the flow over an exponentially stretching sheet with convective thermal condition. *Mathematical Sciences*, 13, 201–211. <https://doi.org/10.1007/s40096-019-0290-8>.
- [47] A. Tanveer & M. B. Ashraf (2023). Mixed convective flow of Sisko nanofluids over a curved surface with entropy generation and Joule heating. *Arabian Journal for Science and Engineering*, 48(9), 11263–11275. <https://doi.org/10.1007/s13369-022-07413-0>.
- [48] C. Tien & Y. C. Yen (1965). The effect of melting on forced convection heat transfer. *Journal of Applied Meteorology (1962-1982)*, 4(4), 523–527.

- [49] N. S. Wahid, N. M. Arifin, I. Pop, N. Bachok & M. E. H. Hafidzuddin (2022). MHD stagnation-point flow of nanofluid due to a shrinking sheet with melting, viscous dissipation and Joule heating effects. *Alexandria Engineering Journal*, 61(12), 12661–12672. <https://doi.org/10.1016/j.aej.2022.06.041>.
- [50] U. Yashkun, K. Zaimi, A. Ishak, I. Pop & R. Sidaoui (2021). Hybrid nanofluid flow through an exponentially stretching/shrinking sheet with mixed convection and Joule heating. *International Journal of Numerical Methods for Heat & Fluid Flow*, 31(6), 1930–1950. <http://dx.doi.org/10.1108/HFF-07-2020-0423>.
- [51] J. K. Zhang, B. W. Li & Y. Y. Chen (2015). The Joule heating effects on natural convection of participating magnetohydrodynamics under different levels of thermal radiation in a cavity. *Journal of Heat Transfer*, 137(5), Article ID: 052502. <https://doi.org/10.1115/1.4029681>.
- [52] K. Zheng, S. I. Shah, M. Naveed Khan, E. Tag-eldin, M. Yasir & A. M. Galal (2023). Numerical simulation of melting heat transfer towards the stagnation point region over a permeable shrinking surface. *Scientia Iranica*, 30(3), 1039–1048. <https://doi.org/10.24200/sci.2022.59956.6518>.